

OPTICAL IMAGE PROCESSING

PACS numbers: 42.55.Kb; 42.30.Ms; 42.30.Wb
DOI: 10.1070/QE2009v039n11ABEH014124

Temporal analysis of the coherent properties of optical images of rough nonplanar objects

V.I. Mandrosov

***Abstract*. The possibility of using temporal analysis to find the relation between chromatic properties of probe radiation and coherent properties of the optical images of rough nonplanar objects is substantiated. The analysis is based on the use of the time correlation function and on the study of the speckle pattern contrast in the optical images. The conditions are determined under which the different parts of the optical image of an object are coherent, partially coherent and incoherent, while probe radiation is manifested as monochromatic, quasi-monochromatic, and polychromatic. It is shown that these conditions depend considerably on the object surface shape. The use of the temporal analysis for three-dimensional imaging of an object by its planar images and improving the optical image quality by removing its speckle pattern is illustrated by examples.**

Keywords: *coherence of optical images, speckles, three-dimensional imaging by the speckle pattern of planar images of objects.*

1. Introduction

Analysis of the coherent properties of optical images of rough objects, including the properties of their speckle patterns, has a long history [1 – 4]. However, the relation between chromatic properties of probe radiation and coherent properties of the optical image was determined only in some particular cases. For example, the contrast of a speckle pattern in the time-averaged intensity distribution $\bar{I} = \langle I \rangle_t$ of the image of a rough nonplanar object was determined as a function of the coherence length L_c of probe radiation in works [4, 5]. The angle brackets $\langle ... \rangle_t$ denote averaging

$$\langle f \rangle_t = \frac{1}{T} \int_{t_0}^{t_0+T} f(t) \mathrm{d}t,$$

where t_0 and T are the initial moment and averaging time, respectively. The approach used in these papers, which is based on the spectral expansion of the modulation function $u(t)$ of probe radiation, allowed the authors to determine this dependence only for Gaussian probe pulses. It was shown that for a fixed coherence length L_c, the speckle pattern contrast in the image of steep slopes of the object surface noticeably exceeds this contrast for the images of smooth slopes.

On the other hand, in [6 – 8] a temporal approach was proposed for determining the relation between chromatic properties of probe radiation and coherent properties of the light fields scattered by objects from the averaged intensity distribution of the scattered field $\bar{I}_{sc} = \langle |E_{sc}|^2 \rangle_t$, where E_{sc} is the field amplitude. This relation is found by using the speckle pattern contrast in the radiation intensity distribution $\bar{I}_{sc}$, which is determined with the help of the time correlation function $B_u(\tau) = \langle u(t)\, u^*(t+\tau) \rangle_t$ {the modulation function was written in the form $u(t) = |u(t)| \exp[\mathrm{i}\psi(t)]$, $\psi(t) = \arctan[\mathrm{Im}\, u(t)/\mathrm{Re}\, u(t)]$ is its phase} under the condition that $B_u(\tau = 0) = 1$ and $T > 10\tau_c$, where

$$\tau_c = \left| \int_{-\infty}^{\infty} B_u(\tau) \mathrm{d}\tau \right|$$

is the coherence time of probe radiation specifying its coherent length $L_c = c\tau_c$ (c is the speed of light).

This approach allows one to determine the speckle pattern contrast for arbitrary temporal structures of probe radiation, including cw radiation and pulsed radiation with pulses of arbitrary shapes. If $\psi(t)$ is a rapidly varying function, it can be described as a random process, which is typical for cw radiation. Then, $\tau_c \approx \tau_\psi/\sigma_\psi$, where τ_ψ and σ_ψ are the correlation time and rms deviation of the phase $\psi(t)$. If $\psi(t)$ is a slowly varying function, which is typical for pulsed radiation, then τ_c is the radiation pulse duration. In [6 – 8], the distinct boundaries are indicated between monochromatic, quasi-monochromatic, and polychromatic probe radiations and between coherent, partially coherent, and incoherent fields scattered by a rough nonplanar object. It is shown that these boundaries are considerably determined by the surface shape of scattering objects and the size of the observed scattering region.

Note also that in [4, 5] the speckle pattern contrast in the intensity distribution of the image of a nonplanar object was calculated by using a single-scale model of its surface inhomogeneities. The surface irregularities of the object surface in this model are its roughnesses. In this case, it was possible to analyse the contrast only for two limiting cases of very large and very small coherence lengths L_c of probe radiation and under the condition that the optical system forming the image can resolve small details of the surface. However, the scattering surface of a real object is

V.I. Mandrosov Moscow Institute of Physics and Technology (State University), Institutskii per. 9, 141700 Dolgoprudnyi, Moscow region, Russia; e-mail: vmandrosov@mail.ru

Received 31 March 2009; revision received 20 July 2009
Kvantovaya Elektronika **39** (11) 1059 – 1067 (2009)
Translated by M.N. Sapozhnikov

two-scale. This means that it consists of large details, each of them containing several small details, which can be discerned in the case of a high enough resolution of the optical system (Fig. 1). The necessity of using the two-scale model of the object surface appears, for example, in determining the speckle pattern contrast in the image of a remote object when the resolution of the optical system is too low to resolve small details of the object.

The aim of this paper is to find the relation between chromatic properties of probe radiation and coherent properties of the optical image. For this purpose, by using first the temporal approach, we determined the speckle structure contrast in the time-averaged intensity distribution $\bar{I}$ of the optical image of a rough nonplanar object taking into account the two-scale model of its scattering surface. Such an approach allows us to determine the dependence of this contrast on the coherence length L_c of probe radiation. Then, we determine from this dependence the conditions under which different parts of the optical image of the object are coherent, partially coherent, and incoherent, while probe radiation is manifested as monochromatic, quasi-monochromatic, and polychromatic. We will show that these conditions strongly depend on the coherence length of probe radiation and the object surface shape. Two methods are presented as the examples of practical application of the temporal approach. The first method involves the three-dimensional imaging of rough nonplanar objects by the speckle pattern contrast in the intensity distribution at different points of their planar images, while the second method is used to improve the image quality of these objects distorted by the high-contrast speckle pattern and is based on the accumulation of their images by probing with several radiation sources.

2. Analysis of the field distribution in optical images of rough nonplanar objects in the two-scale model of their surfaces

Let us determine the field distribution in the plane of the optical image of a rough nonplanar object within the framework of the two-scale model of its surface consisting, as mentioned above, of large and small details (Fig. 1). The radius vector of the surface is $\boldsymbol{r}_\Sigma = \boldsymbol{r} + \boldsymbol{N}_\xi(\boldsymbol{r})\xi(\boldsymbol{r})$, where $\boldsymbol{r}(x, y, z)$ is the radius vector of the surface formed by small details; $\xi(\boldsymbol{r})$ and $\boldsymbol{N}_\xi(\boldsymbol{r})$ are the distribution of roughness heights (small-scale irregularities) on this surface and the normal to it, respectively. In addition, $\boldsymbol{r} = \boldsymbol{r}_m + \boldsymbol{N}_\eta(\boldsymbol{r})\eta(\boldsymbol{r})$, where $\eta(\boldsymbol{r})$ and $\boldsymbol{N}_\eta(\boldsymbol{r})$ are the height distribution for large-

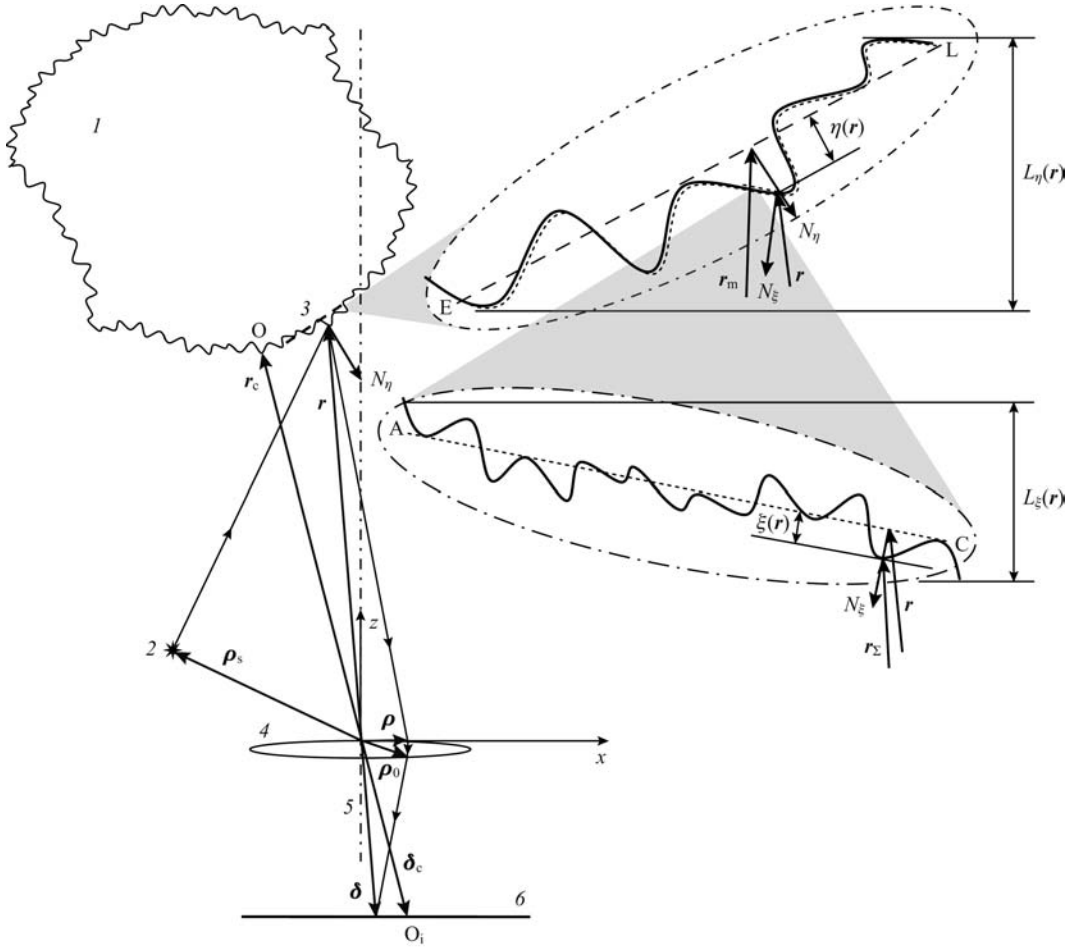

Figure 1. Formation of the object image in the two-scale model of the object surface:
(*1*) object; (*2*) probe source; (*3*) small scattering region; (*4*) imaging optical system; (*5*) optical axis; (*6*) object image plane; at the top right is presented the magnified image of region *3*, at the bottom left – the object surface profile even at a larger magnification; the thin wavy lines around straight lines AC and EL show the height distributions of the object surface roughness; the arrows denote the path of one light beam from the source to the object surface and further from the object surface to the optical system, inside and from it to the object image pane.

scale irregularities consisting of small details and the normal to the average surface of the object, respectively; and $\boldsymbol{r}_{\mathrm{m}}$ is the radius vector of the intersection point of the normal $\boldsymbol{N}_{\eta}(\boldsymbol{r})$ with the average surface. We will assume below that roughnesses $\xi(\boldsymbol{r})$ and large-scale irregularities $\eta(\boldsymbol{r})$ are distributed according to the Gaussian law with the correlation radii ℓ_{ξ} and $\ell_{\eta} \gg \ell_{\xi}$ and rms deviations $\sigma_{\xi} = (\langle \xi^2(\boldsymbol{r}) \rangle_{\xi})^{1/2}$ and $\sigma_{\eta} = (\langle \eta^2(\boldsymbol{r}) \rangle_{\eta})^{1/2} \gg \sigma_{\xi}$ [angle brackets $\langle ... \rangle_{\xi}$ and $\langle ... \rangle_{\eta}$ denote averaging by the different realisations of roughnesses $\xi(\boldsymbol{r})$ and large-scale irregularities $\eta(\boldsymbol{r})$ of the object surface]. The parameters l_{η} and σ_{ξ} can be treated as the average length and average height, respectively, of small details. We assume that $\sigma_{\xi} \gg \lambda_0$, where $\lambda_0 = \omega_0/c$ is the mean radiation frequency. We also assume that the object is probed with a point source with the emission field amplitude $E_z(t) = E_{\mathrm{s}} U(t)$, where E_{s} is the field amplitude on the source aperture and $U(t) = u(t)\exp(\mathrm{i}\omega_0 t)$. By using the results from [6, 7], we can show the field in the image plane is described in the Kirchhoff approximation by the expression

$$E(\boldsymbol{\delta}, t, \boldsymbol{\rho}_{\mathrm{s}}) \sim [E_{\mathrm{s}}/(\lambda_0 r_{\mathrm{c}} S_{\rho})]$$

$$\times \iint k(\boldsymbol{r}_{\Sigma}) \Lambda(\boldsymbol{\rho}) U[t - \Psi(\boldsymbol{r}_{\Sigma}, \boldsymbol{\rho}, \boldsymbol{\delta})/c] \, \mathrm{d}\boldsymbol{\rho} \, \mathrm{d}\boldsymbol{r}_{\Sigma}, \qquad (1)$$

where $k(\boldsymbol{r}_{\Sigma})$ is the reflectance distribution on the object surface; S_{ρ} is the entrance pupil area of the imaging optical system; $\Lambda(\boldsymbol{\rho})$ is the system pupil function; $\boldsymbol{\rho}$ is the radius vector at the entrance pupil of the recording system; $\boldsymbol{r}_{\mathrm{c}}$ is the radius vector of the object surface point O nearest to the centre;

$$\Psi_0(\boldsymbol{r}_{\Sigma}, \boldsymbol{\rho}, \boldsymbol{\delta}) = |\boldsymbol{r}_{\Sigma} - \boldsymbol{\rho}_{\mathrm{s}}| + |\boldsymbol{r}_{\Sigma} - \boldsymbol{\rho}|$$

$$+ \Psi_{\mathrm{i}}(\boldsymbol{\rho}) + |\boldsymbol{\delta} - \boldsymbol{\rho}_0| \qquad (2)$$

is the optical path of the probe radiation beam from the source to the image plane; $\boldsymbol{\rho}_{\mathrm{s}}$ is the radius vector of the probe radiation source; $\boldsymbol{\delta}$ is the radius vector of a point in the image plane; $\Psi_{\mathrm{i}}(\boldsymbol{\rho})$ is the optical path of the probe beam between the entrance and exit pupils of the optical system; and $\boldsymbol{\rho}_0$ is the radius vector of the point at which the beam escapes from the optical system.

As a rule, the axis of the optical system is oriented to the object and its entrance pupil is circular, so that $S_{\rho} = \pi d_{\rho}^2$, where d_{ρ} is the entrance pupil diameter (Fig. 2). Then, $r_{\mathrm{c}} \approx z_0$, where z_0 is the distance between the object and the entrance pupil, and the modulus of the radius vector of point $\mathrm{O_i}$ corresponding to the point O of the object is $\delta_{\mathrm{c}} \approx z_{\mathrm{i}}$, where z_{i} is the distance between the exit pupil of the optical system and the image plane. Usually, $\Psi_{\mathrm{i}}(\boldsymbol{\rho}) \approx C_0 - \rho^2/(2f)$, where C_0 is a constant determined by the design of the imaging optical system, and f is its focal distance. For example, if the system is a thin plano-convex lens with the radius R of a spherical convex surface and the refractive index n (Fig. 2), then in the paraxial approximation $f = R/[2(n-1)]$ and $C_0 \approx Hn$, where $H \approx |\boldsymbol{\rho} - \boldsymbol{\rho}_0|$ is the distance between the entrance and exit pupils of the optical system.

We will analyse relation (1) by assuming that $z_0 \gg d$, where $d \approx \rho_0[\sigma_{\xi}/(2\ell_{\xi})]^2$ is the transverse size of the backscattering region of the object [6]. Then, in the Fresnel approximation, taking into account relations (1), (2), and

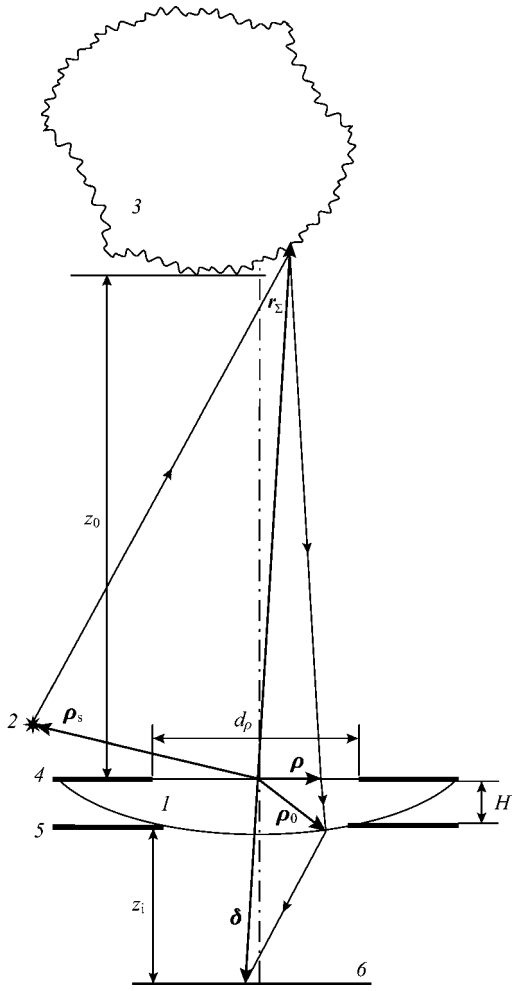

Figure 2. To the calculation of the optical path of beams forming the object image by means of a plano-convex lens:
(*1*) plano-convex lens; (*2*) probe source; (*3*) probed object; (*4*, *5*) entrance and exit pupil planes; (*6*) object image plane.

the lens formula $1/z_0 + 1/z_{\mathrm{i}} = 1/f$, the field distribution in the object image with an accuracy to insignificant factors and small terms is described by the expression

$$E(\boldsymbol{\delta}, t, \boldsymbol{\rho}_{\mathrm{s}}) \sim (E_{\mathrm{s}}/S_{\rho}) \iint k(\boldsymbol{r}) \Lambda(\boldsymbol{\rho}) U\{t - [2r + \boldsymbol{r}\boldsymbol{\rho}_{\mathrm{s}}/z_0$$

$$+ q_N \xi(\boldsymbol{r}) + \boldsymbol{\rho}(\boldsymbol{r}/z_0 + \boldsymbol{\delta}/z_{\mathrm{i}})]/c\} \, \mathrm{d}\boldsymbol{\rho} \, \mathrm{d}\boldsymbol{r},$$

where $q_N = \boldsymbol{q}\boldsymbol{N}_{\xi}(\boldsymbol{r})$ and $\boldsymbol{q} \approx 2\boldsymbol{r}_{\mathrm{c}}/r_{\mathrm{c}}$ is the scattering vector. For the case most often encountered in practice, when $L_{\mathrm{c}} \gg \sigma_{\xi}$, by taking into account that $r_{\mathrm{c}} \approx z_0$, we obtain in the Fresnel approximation:

$$E(\boldsymbol{\delta}, t, \boldsymbol{\rho}_{\mathrm{s}}) \sim [\exp(\mathrm{i}\omega_0 t) E_{\mathrm{s}}/(\lambda_0 z_0 S_{\rho})] \iint k(\boldsymbol{r}) \Lambda(\boldsymbol{\rho})$$

$$\times \exp\{2\pi\mathrm{i}[2r + \boldsymbol{r}\boldsymbol{\rho}_{\mathrm{s}}/z_0 + q_N \xi(\boldsymbol{r})$$

$$+ \boldsymbol{\rho}(\boldsymbol{r}/z_0 + \boldsymbol{\delta}/z_{\mathrm{i}})]/\lambda_0\} \, u\{t - [2r + \boldsymbol{r}\boldsymbol{\rho}_{\mathrm{s}}/z_0$$

$$+ \boldsymbol{\rho}(\boldsymbol{r}/z_0 + \boldsymbol{\delta}/z_{\mathrm{i}})]/c\} \mathrm{d}\boldsymbol{\rho} \, \mathrm{d}\boldsymbol{r}. \qquad (3)$$

Let us expand the function u in (3) as a power series in the radius vector $\boldsymbol{\rho}$. By integrating relation (3) with respect to $\boldsymbol{\rho}$, we obtain

$$E(\boldsymbol{\delta}, t, \boldsymbol{\rho}_s) = E_i(\boldsymbol{\delta}, t, \boldsymbol{\rho}_s) + E_a(\boldsymbol{\delta}, t, \boldsymbol{\rho}_s), \tag{4}$$

where

$$E_i(\boldsymbol{\delta}, t, \boldsymbol{\rho}_s) \sim [\exp(i\omega_0 t)E_s/(\lambda_0 z_0)] \int k(\boldsymbol{r})h(\boldsymbol{r}, \boldsymbol{\delta})$$

$$\times \exp\{-2\pi i[2r + \boldsymbol{r}\boldsymbol{\rho}_s/z_0 + q_N\xi(\boldsymbol{r})]/\lambda_0\}$$

$$\times u[t - (2r + \boldsymbol{r}\boldsymbol{\rho}_s/z_0)/c]\, d\boldsymbol{r};$$

$h(\boldsymbol{r}, \boldsymbol{\delta}) = (1/S_\rho) \int \Lambda(\boldsymbol{\rho}) \exp[(2\pi i/z_0)\boldsymbol{\rho}(\boldsymbol{r} + \mu\boldsymbol{\delta})]d\boldsymbol{\rho}$ is the pulse response of the imaging optical system; $\mu = z_0/z_i$ is the scale factor; and $E_a(\boldsymbol{\delta}, t, \boldsymbol{\rho}_s) \sim (\lambda_0/L_c)E_i(\boldsymbol{\delta}, t, \boldsymbol{\rho}_s)$. The resolution of the optical system is determined by the width $\Delta_r = [\int h(\boldsymbol{r}, \boldsymbol{\delta})\, d\boldsymbol{r}]^{1/2} \approx z_0\lambda_0/d_\rho$ of the pulsed response $h(\boldsymbol{r}, \boldsymbol{\delta})$ along the radius vector $\boldsymbol{r}$. It is equal to the size of the projection of the minimal resolvable site of the object surface on the image plane and is often called a resolution element in the literature [5] (Figs 3 and 4). Note that when the resolution of the optical system is very high and the entrance pupil diameter d_ρ is so large that $\Delta_r < \lambda_0(\sigma_\xi/\ell_\xi)$, the relation $E(\boldsymbol{\delta}, t, \boldsymbol{\rho}_s) \sim k(\boldsymbol{r} = -\mu\boldsymbol{\delta})$ is fulfilled [4]. This means that the field distribution in the image is the exact copy of the distribution of the reflectance $k(\boldsymbol{r})$ on the object surface.

3. Contrast of a speckle pattern in the intensity distribution of images of rough nonplanar objects and coherent properties of these images

Let us determine now the speckle pattern contrast $C(\boldsymbol{\delta})$ in the time-averaged random intensity distribution

$$\bar{I}(\boldsymbol{\delta}) = \frac{1}{T}\int_{t_0}^{t_0+T} |E(\boldsymbol{\delta}, t, \boldsymbol{\rho}_s)|^2 dt$$

of the field $E(\boldsymbol{\delta}, t)$ in the image of an object taking into account the two-scale nature of its surface. The contrast $C(\boldsymbol{\delta})$ is determined from different expressions depending on the resolution of the imaging optical system. If $\ell_\eta \gg \Delta_r$, small details on the object surface, which represent large-scale irregularities $\eta(\boldsymbol{r})$ of its surface, are resolved by this system. Then, $C(\boldsymbol{\delta}) = C_\xi(\boldsymbol{\delta}) = \langle \bar{I}^2(\boldsymbol{\delta})\rangle_\xi / \langle \bar{I}(\boldsymbol{\delta})\rangle_\xi^2 - 1$. According to calculations presented in Appendix,

$$C_\xi(\boldsymbol{\delta}) = \frac{[L_c\Delta_r^2/L_\xi(\boldsymbol{\delta})] \int k_\xi^2(\boldsymbol{r})|h(\boldsymbol{r}, \boldsymbol{\delta})|^4 d\boldsymbol{r}}{[\int k_\xi(\boldsymbol{r})|h(\boldsymbol{r}, \boldsymbol{\delta})|^2 d\boldsymbol{r}]^2}. \tag{5}$$

For the coherence length of probe radiation $L_c \gg L_\xi(\boldsymbol{\delta})$, we obtain $C(\boldsymbol{\delta}) = C_\xi(\boldsymbol{\delta}) = 1$.

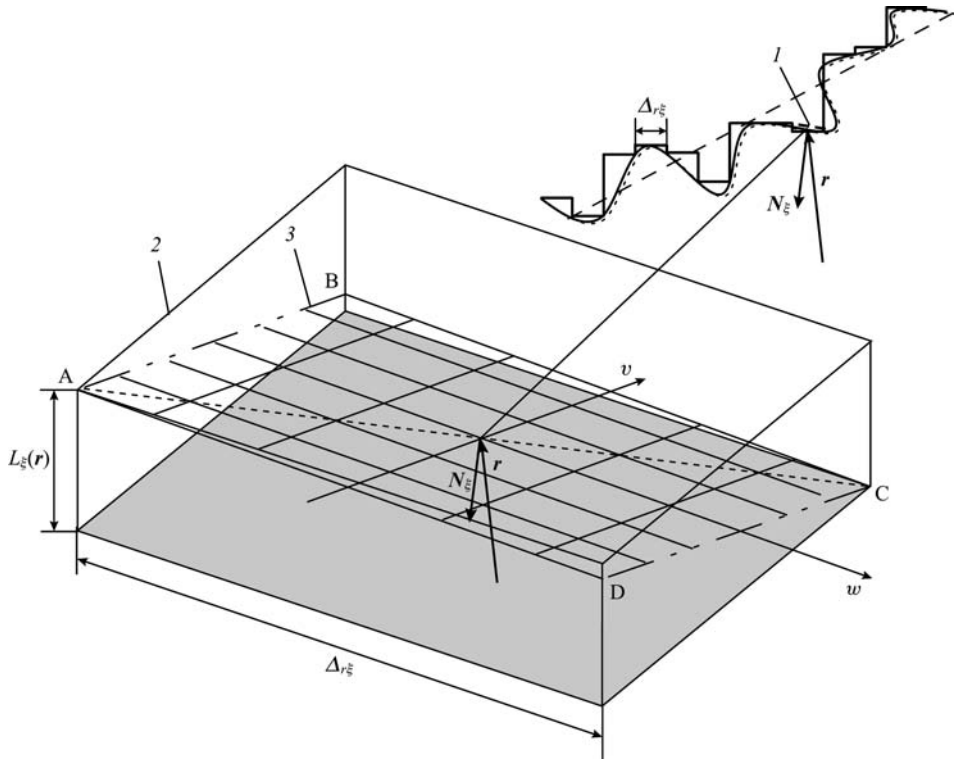

Figure 3. Detailed stepwise approximation of the object surface by parallelepipeds of height $L_\xi(\boldsymbol{r} = -\mu\boldsymbol{\delta})$ and square bases with side $\Delta_{r\xi}$ in the case of a high-resolution imaging system:
(*1*) small region of the object; (*2*) parallelepiped approximating this region; (*3*) parallelogram ABCD tangential to the object surface; w and v are the axes of the local coordinate system; sides AB and CD lie on the bases of the approximating parallelepiped.

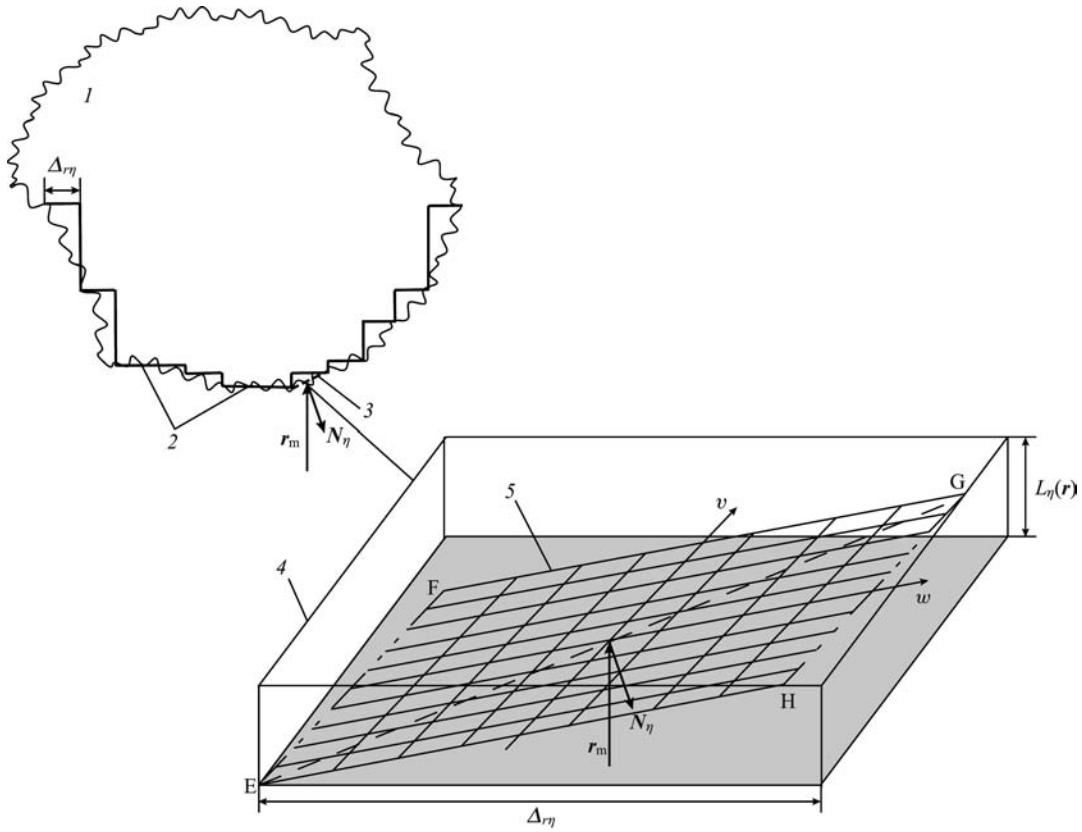

Figure 4. Rough stepwise approximation of the object surface by parallelepipeds of height $L_\eta(\boldsymbol{r} = -\mu\boldsymbol{\delta})$ and square bases with side $\Delta_{r\eta}$ in the case of a low-resolution imaging system:
(*1*) probed object; (*2*) object surface regions in which $L_\eta(\boldsymbol{r}) = 0$ (these regions are parallel to the entrance pupil plane of the optical system, and for this reason the speckle contrast in their images is close to unity); (*3*) object surface region shown in Fig. 1; (*4*) parallelepiped approximating region (*3*); (*5*) parallelogram EFGH tangential to the average object surface; w and v are the axes of the local coordinate system; sides EF and GH lie on the bases of the approximating parallelepiped.

If $\ell_\eta \ll \Delta_r$, the optical system cannot resolve small details of the object surface. Then, $C(\boldsymbol{\delta}) = C_\eta(\boldsymbol{\delta}) = \langle\langle \bar{I}^2(\boldsymbol{\delta})\rangle_\xi\rangle_\eta / \langle\langle \bar{I}(\boldsymbol{\delta})\rangle_\xi\rangle_\eta^2 - 1$. Taking into account that the distribution of the field $E(\boldsymbol{\delta}, t)$ is described by a Gaussian, we obtain the relation

$$C_\eta(\boldsymbol{\delta}) = \frac{1}{T^2}\int_{t_0}^{t_0+T}\int_{t_0}^{t_0+T} |\langle\langle E(\boldsymbol{\delta}, t_1)E^*(\boldsymbol{\delta}, t_2)\rangle_\xi\rangle_\eta|^2 \mathrm{d}t_1\mathrm{d}t_2 \times \left(\langle\langle \bar{I}(\boldsymbol{\delta})\rangle_\xi\rangle_\eta^2\right)^{-1},$$

which resembles expression (A1) in Appendix. Taking relation (A3) into account, we can show that

$$C_\eta(\boldsymbol{\delta}) = \frac{L_c\Delta_r^2 \int\langle(1/q_\xi)k_\xi^2(\boldsymbol{r})\rangle_\eta |h(\boldsymbol{r}, \boldsymbol{\delta})|^4 \mathrm{d}\boldsymbol{r}}{[\int\langle k_\xi(\boldsymbol{r})\rangle_\eta |h(\boldsymbol{r}, \boldsymbol{\delta})|^2 \mathrm{d}\boldsymbol{r}]^2}. \quad (6)$$

To analyse expression (6), we approximate a small site of the mean surface of the object by a plane (Fig. 4). This plane almost coincides with the EFGH plane, which is tangential to this site at its centre determined by the radius vector $\boldsymbol{r}_m$. The plane is oriented perpendicular to the normal $\boldsymbol{N}_\eta(\boldsymbol{r})$ to the mean surface of the object. Expression (6) depends on the function $q_\xi(\boldsymbol{r}) = q_\perp(\boldsymbol{r})/q_N(\boldsymbol{r})$ equal to the slope of a tangent to the object surface, which is a random quantity determined by the derivatives from the height distribution for large-scale irregularities. Therefore, averaging over $\eta(\boldsymbol{r})$ can be replaced by averaging over q_ξ. This means that the relations

$$\langle(1/q_\xi)k_\xi^2(\boldsymbol{r})\rangle_\eta = \int (1/q_\xi)k_\xi^2(\boldsymbol{r})W(q_\xi)\mathrm{d}q_\xi,$$
$$\langle k_\xi(\boldsymbol{r})\rangle_\eta = \int k_\xi(\boldsymbol{r})W(q_\xi)\mathrm{d}q_\xi \quad (7)$$

take place, where $W(q_\xi)$ is the probability density distribution of the function $q_\xi(\boldsymbol{r})$. Taking into account that the distribution of heights is described by a Gaussian, we can show that $W(q_\xi) = (\ell_\eta/\sigma_\eta)\exp[-\ell_\eta^2(q_\xi - q_\eta)^2/\sigma_\eta^2]$, where $q_\eta = \widetilde{q}_\perp/\widetilde{q}_N = \langle q_\xi\rangle_\eta$; $\widetilde{q}_\perp \approx (4 - \widetilde{q}_N^2)^{1/2}$; and $\widetilde{q}_N = \boldsymbol{q}\boldsymbol{N}_\eta(\boldsymbol{r})$. For the coherence length of probe radiation $L_c \ll L_\eta(\boldsymbol{\delta}) = \Delta_r q_\eta$, where $L_\eta(\boldsymbol{\delta})$ is the length of the projection of the EFGH plane on the vector $\boldsymbol{q}$ (see Figs. 1 and 4), taking into account expressions (6) and (7) and the relation $\sigma_\eta/\ell_\eta \ll \sigma_\xi/\ell_\xi$, which is usually fulfilled, we obtain

$$C_\eta(\boldsymbol{\delta}) = \frac{[L_c\Delta_r^2/L_\eta(\boldsymbol{\delta})]\int k_\eta(\boldsymbol{r})|h(\boldsymbol{r}, \boldsymbol{\delta})|^4 \mathrm{d}\boldsymbol{r}}{[\int k_\eta(\boldsymbol{r})|h(\boldsymbol{r}, \boldsymbol{\delta})|\,\mathrm{d}\boldsymbol{r}]^2}, \quad (8)$$

where $k_\eta(\boldsymbol{r}) \approx (\ell_\xi/\sigma_\xi)^2 k_i(\boldsymbol{r})\exp(-q_\eta\ell_\xi/\sigma_\xi)^2$ and $k_i(\boldsymbol{r}) = |k(\boldsymbol{r})|^2$. For the coherence length $L_c \gg L_\eta(\boldsymbol{\delta})$, we have $C_\eta(\boldsymbol{\delta}) \approx 1$. Relations (5) and (8) can be simplified, taking into account that

$$\Delta_r \ll \Lambda_x = k_i(\boldsymbol{r} = -\mu\boldsymbol{\delta})/[\partial^2 k_i(\boldsymbol{r} = -\mu\boldsymbol{\delta})/\partial^2 x]^{1/2},$$
$$\Delta_r \ll \Lambda_y = k_i(\boldsymbol{r} = -\mu\boldsymbol{\delta})/[\partial^2 k_i(\boldsymbol{r} = -\mu\boldsymbol{\delta})/\partial^2 y]^{1/2}, \quad (9)$$

where Λ_x and Λ_y are the characteristic sizes of the details of distribution (8) along the x and y axes [4]. Then,

$$\langle \bar{I}(\boldsymbol{\delta})\rangle_\xi \sim k_\xi(\boldsymbol{r} = -\mu\boldsymbol{\delta}) \int |h(\boldsymbol{r}, \boldsymbol{\delta})|^2 \mathrm{d}\boldsymbol{r}$$
$$\approx \Delta_r^2 k_\xi(\boldsymbol{r} = -\mu\boldsymbol{\delta}), \quad (10)$$

$$\frac{1}{T^2}\int_{t_0}^{t_0+T}\int_{t_0}^{t_0+T} |\langle E(\boldsymbol{\delta}, t_1)E^*(\boldsymbol{\delta}, t_2)\rangle_\xi|^2 \mathrm{d}t_1 \mathrm{d}t_2$$
$$\sim [k_\xi(\boldsymbol{r} = -\mu\boldsymbol{\delta})]^2 \int |h(\boldsymbol{r}, \boldsymbol{\delta})|^4 \mathrm{d}\boldsymbol{r}$$
$$\approx [\Delta_r^4 L_c/L_\xi(\boldsymbol{\delta})][k_\xi(\boldsymbol{r} = -\mu\boldsymbol{\delta})]^2. \quad (11)$$

Taking relations (9), (10), and (11) into account under the condition that $L_c \ll L_\xi(\boldsymbol{\delta}), L_\eta(\boldsymbol{\delta})$, we obtain

$$C_\xi(\boldsymbol{\delta}) \approx L_c/L_\xi(\boldsymbol{\delta}) \ll 1,\ C_\eta(\boldsymbol{\delta}) \approx L_c/L_\eta(\boldsymbol{\delta}) \ll 1. \quad (12)$$

Such small contrasts can be physically explained as follows (see also section 3.6 in [4]). Let us fix a small region of the object image corresponding to the minimal resolvable part of the object surface. Then, we divide mentally this region by planes parallel to the entrance pupil plane and separated by distances L_c. As a result, the region will be divided into $N_\xi \approx L_\xi(\boldsymbol{\delta})/L_c \gg 1$ sites in the case of high resolution and into $N_\eta \approx L_\eta(\boldsymbol{\delta})/L_c \gg 1$ sites in the case of low resolution. The fields scattered by these sites make N_ξ or N_η statistically independent contributions to the formation of the fixed region of the image. Therefore, the contrast in this region will be inversely proportional to either N_ξ or N_η.

Let us estimate now the dependence of the contrast $C_\xi(\boldsymbol{\delta})$ on the coherence length for arbitrary ratios L_c/L_ξ for imaging optical systems with the high resolution, when $\Delta_r \ll \ell_\eta$. In this case, taking into account relations (A1), (A3), (9), (10), and (11), we have

$$C_\xi(\boldsymbol{\delta}) = \frac{\iint |h(\boldsymbol{r}_1, \boldsymbol{\delta})h^*(\boldsymbol{r}_2, \boldsymbol{\delta})|^2 |B_u[\beta(\boldsymbol{r}_1, \boldsymbol{r}_2)]|^2 \mathrm{d}\boldsymbol{r}_1 \mathrm{d}\boldsymbol{r}_2}{[\int |h(\boldsymbol{r}, \boldsymbol{\delta})|^2 \mathrm{d}\boldsymbol{r}]^2}. \quad (13)$$

Taking into account that $\beta(\boldsymbol{r}_1, \boldsymbol{r}_2) \approx [2q_\xi(w_1 - w_2)]/L_c$, by approximating the functions h and B_u by Gaussians, $h(\boldsymbol{r}, \boldsymbol{\delta}) \approx \exp\{-[(w + \mu\delta_x/z_i)^2 + (v + \mu\delta_y/z_i)^2]/\Delta_\xi^2\}$ and $B_u[\beta(\boldsymbol{r}_1, \boldsymbol{r}_2)] \approx \exp[-2q_\xi(w_1 - w_2)^2/L_c^2]$, and replacing integration with respect to $\boldsymbol{r}$ in (13) by integration with respect to w and v in the interval $[-\infty, \infty]$, we obtain $C(\boldsymbol{\delta}) = C_\xi(\boldsymbol{\delta}) \approx [1 + \alpha_\xi(L_c/L_\xi)^2]^{1/2}$, where $\alpha_\xi \approx 1$. For $L_c \gg L_\xi$, the contrast is $C(\boldsymbol{\delta}) = C_\xi(\boldsymbol{\delta}) \approx 1$, and for $L_c \ll L_\xi$, we have $C(\boldsymbol{\delta}) = C_\xi(\boldsymbol{\delta}) \approx L_c/L_\xi(\boldsymbol{\delta})$. Similarly in the case of a low resolution, when $\ell_\eta \ll \Delta_r$, the contrast is $C(\boldsymbol{\delta}) = C_\eta(\boldsymbol{\delta}) \approx [1 + \alpha_\eta(L_c/L_\eta)^2]^{1/2}$, where $\alpha_\eta \approx 1$. In this case, for $L_c \gg L_\eta$, the contrast is $L_c \gg L_\eta$, and for $L_c \ll L_\eta$, we have $C(\boldsymbol{\delta}) = C_\eta(\boldsymbol{\delta}) \approx L_c/L_\eta(\boldsymbol{\delta})$.

Let us use the results obtained above to classify the chromatic properties of probe radiations and coherent properties of optical images, similarly to the classification proposed in paper [6]. When the coherence length L_c of probe radiation exceeds the thickness L_s of the backscattering region, this radiation scattered from the entire object behaves as monochromatic radiation and its image as a whole manifests itself as a coherent image. If $L_c \leqslant L_s$, the chromatic properties of probe radiations and coherent properties of optical images are determined by the resolution of the imaging optical system and the steepness of the slopes of the object surface.

In the images of the smooth slopes of the object surface on which $L_\xi(\boldsymbol{\delta}) \ll L_c$ at high resolution and $L_\eta(\boldsymbol{\delta}) \ll L_c$ at low resolution, the contrast of the time-averaged intensity distribution is $C_\xi(\boldsymbol{\delta}) = C_\eta(\boldsymbol{\delta}) \approx 1$. Therefore, the probe radiation scattered by these slopes behaves as monochromatic radiation, while the images of smooth slopes manifest themselves as coherent images. In the images of steep slopes of the object surface on which $C_\xi(\boldsymbol{\delta}) \approx L_c/L_\xi(\boldsymbol{\delta}) \ll 1$ at high resolution ($L_\xi(\boldsymbol{\delta}) \gg L_c$) and $C_\eta(\boldsymbol{\delta}) \approx L_c/L_\eta(\boldsymbol{\delta}) \ll 1$ at low resolution ($L_\eta(\boldsymbol{\delta}) \gg L_c$), the probe radiation scattered by these slopes behaves as polychromatic radiation, and the images of steep slopes manifest themselves as incoherent images. In the intermediate case between smooth and steep slopes for the high $[0.25L_c \geqslant L_\xi(\boldsymbol{\delta}) \geqslant 0.1L_c]$ and low $[0.25L_c \geqslant L_\eta(\boldsymbol{\delta}) \geqslant 0.1L_c]$ resolutions, the contrast of the time-averaged intensity distribution is $C(\boldsymbol{\delta}) \sim 1$. This means that probe radiation behaves as quasi-monochromatic radiation, while the images of these intermediate slopes manifest themselves as partially coherent images.

Thus, if $L_c \leqslant L_s$, the coherent properties of different regions of the same optical image of a nonplanar rough object strongly depend on the steepness of different regions of its surface. This is demonstrated in Fig. 4 showing the two smooth regions of the object surface on which $L_\eta(\boldsymbol{\delta}) \approx 0$. Their images are the coherent regions of the object image. Region (*3*) of the object surface is an example of the intermediate case. Its image is one of the partially coherent regions of the object image.

4. Three-dimensional imaging by the planar optical image of an object by using the temporal approach

Let us use relations (15) for the three-dimensional imaging of an object by the contrast of a speckle pattern in each region of its planar image. If the resolution of the imaging optical system is high and $\ell_\eta \gg \Delta_r$, we can perform a detailed stepwise approximation of the object surface with the help of parallelepipeds with square bases with the side $\Delta_{r\xi} = \lambda_0 z_0/d_{\rho\xi}$ (where $d_{\rho\xi}$ is the entrance pupil diameter of this system) and height $L_\xi(\boldsymbol{\delta}) \approx L_c/C_\xi(\boldsymbol{\delta})$ (see Fig. 3). If the resolution of the optical system is low and $\ell_\eta \ll \Delta_r$, we can perform a rough step approximation of this surface with the help of parallelepipeds with square bases with the side $\Delta_{r\eta} = \lambda_0 z_0/d_{\rho\eta} \gg \Delta_{r\xi}$ (where $d_{\rho\eta} \ll d_{\rho\xi}$ is the entrance pupil diameter of this system) and height $L_\eta(\boldsymbol{\delta}) \approx L_c/C_\eta(\boldsymbol{\delta})$ (see Fig. 4).

The contrast $C(\boldsymbol{\delta})$ at each point of the object image can be determined with the help of several (no more than a hundred) probe sources arranged in the form of an array in the entrance pupil plane (Fig. 5). Let us denote the radius vector of the mnth source as $\boldsymbol{\rho}_{smn}$, where m and n are the array line and column numbers, respectively. We recorded N images with the intensity distributions $\bar{I}(\boldsymbol{\delta}, \boldsymbol{\rho}_{smn})$ in each

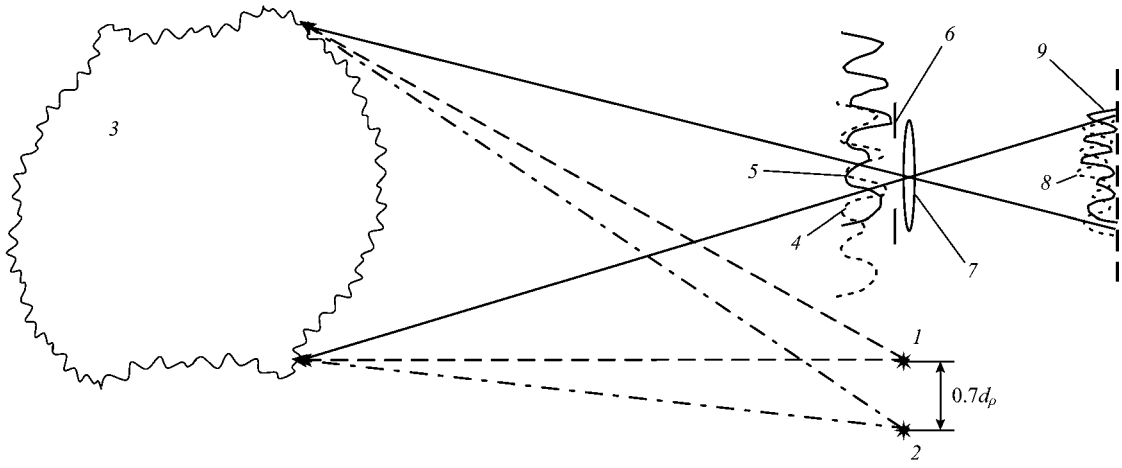

Figure 5. Descriptive interpretation of the statistical independence of object images formed by two probe radiation sources separated by a distance of $0.7d_\rho$:
(*1*, *2*) probe radiation sources; (*3*) rough object; (*4*, *5*) speckles formed by probe radiation from sources (*1*) and (*2*), respectively, scattered by entrance pupil (*6*) of imaging optical system (*7*); (*8*, *9*) coherent statistically independent object images corresponding to them.

of them. When the distance between adjacent sources is no less than $0.7d_\rho$, these images are so separated that their realisations on the entrance pupil are completely discernible: $\langle \bar{I}(\boldsymbol{\delta}, \boldsymbol{\rho}_{\mathrm{s}m_1n_1})\bar{I}(\boldsymbol{\delta}, \boldsymbol{\rho}_{\mathrm{s}m_2n_2})\rangle_\xi = \delta_{m_1n_1,m_2n_2}$ (δ is the Kronecker delta) [4, 5] (Fig. 6). Then, the approximate contrast value is calculated from the expression $C_{\mathrm{i}}(\boldsymbol{\delta}) = \langle \bar{I}^2(\boldsymbol{\delta})\rangle_{\mathrm{i}}/\langle \bar{I}(\boldsymbol{\delta})\rangle_{\mathrm{i}}^2 - 1$, where $\langle \bar{I}^2(\boldsymbol{\delta})\rangle_{\mathrm{i}} = N^{-1}\sum \bar{I}^2(\boldsymbol{\delta}, \boldsymbol{\rho}_{\mathrm{s}mn})$; $\langle \bar{I}(\boldsymbol{\delta})\rangle_{\mathrm{i}} = N^{-1}\sum \bar{I}(\boldsymbol{\delta}, \boldsymbol{\rho}_{\mathrm{s}mn})$ (summation is performed over all the sources). In the case of the detailed stepwise approximation, it is expedient to have no less than 50 sources. Then, $C_{\mathrm{i}}(\boldsymbol{\delta}) = C_\xi(\boldsymbol{\delta})$ with an accuracy of 2 %. In the case of the rough stepwise approximation of the object surface, it is sufficient to have no more than 20 sources (Fig. 6). Then, $C_{\mathrm{i}}(\boldsymbol{\delta}) = C_\eta(\boldsymbol{\delta})$ with an accuracy of up to 5 %.

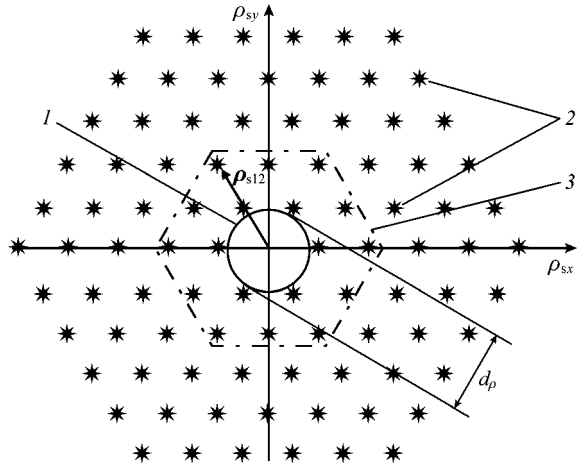

Figure 6. Compact arrangement of probe radiation sources around the entrance pupil of the optical system: (*1*) entrance pupil; (*2*) probe radiation sources; (*3*) hexagonal region restricted by the dot-and-dash line in which the sources are located, their number being sufficient for determining the speckle contrast in the plane image of the object in the case of the rough stepwise approximation of its surface.

5. Improvement of the quality of the optical image of a nonplanar object by accumulating its statistically independent images

It is known that the speckle pattern of the image of a rough object with the contrast $C(\boldsymbol{\delta}) > 0.1$ noticeably deteriorates the quality of this image [1 – 5]. Speckles are most clearly observed in the images of object regions that are parallel to the entrance pupil plane of the optical system (Fig. 4). In this regions, $L_{\mathrm{c}} \gg L_\eta(\boldsymbol{\delta})$ in the case of poor resolution and $L_{\mathrm{c}} \gg L_\xi(\boldsymbol{\delta})$ for good resolution. Under these conditions, the contrast is $C(\boldsymbol{\delta}) \approx 1$.

The quality of the optical image of a nonplanar object can be improved by summing (accumulating) its statistically independent images formed by probing the object simultaneously with several sources. This takes place when the distance between adjacent sources is no less than $0.7d_\rho$ (Fig. 5). In the case of the most compact arrangement of sources separated by a distance of $0.7d_\rho$ in the array (Fig. 6), the intensity distribution in the accumulated image is $\langle \bar{I}(\boldsymbol{\delta})\rangle_{\mathrm{i}} = N^{-1}\sum \bar{I}(\boldsymbol{\delta}, \boldsymbol{\rho}_{\mathrm{s}mn})$. The contrast of the speckle pattern in this image achieved due to the accumulation of statistically independent images is considerably lower than the contrast of the speckle pattern in the image obtained by using one source. Such a low contrast provides the high quality of the accumulated image $\langle \bar{I}(\boldsymbol{\delta})\rangle_{\mathrm{i}}$. The integral criterion of quality, we can use the correlation criterion $K = \int \bar{I}_{\mathrm{i}}(\boldsymbol{\delta})\langle \bar{I}(\boldsymbol{\delta}, \boldsymbol{\rho}_{\mathrm{s}m_0n_0})\rangle_\xi \,\mathrm{d}\boldsymbol{\delta} / \int \langle \bar{I}(\boldsymbol{\delta}, \boldsymbol{\rho}_{\mathrm{s}m_0n_0})\rangle_\xi^2 \,\mathrm{d}\boldsymbol{\delta}$ [4] of the closeness of this image to the ideal image representing the intensity distribution $\langle \bar{I}(\boldsymbol{\delta}, \boldsymbol{\rho}_{\mathrm{s}m_0n_0})\rangle_\xi$ in the initial image averaged over the roughnesses of the object surface. The efficiency η_{c} of this criterion or, in other words, the approximation accuracy of the ideal image of the object by the accumulated image $\langle \bar{I}(\boldsymbol{\delta})\rangle_{\mathrm{i}}$ is determined by the relative fluctuations of K: $\eta_{\mathrm{c}} = (\langle K^2\rangle - \langle K\rangle^2)/\langle K\rangle^2$. By using the temporal approach and the approach used to calculate the parameter η_{c} in papers [4, 5], we can show that for arbitrary coherent lengths of sources, the relative fluctuation is $\eta_{\mathrm{c}} \approx C_{\mathrm{a}}(\boldsymbol{\delta})/(MN)$, where M is the number of spots; $C_{\mathrm{a}}(\boldsymbol{\delta}) = \int C(\boldsymbol{\delta})\,\mathrm{d}\boldsymbol{\delta}/S_{\mathrm{i}}$ is the average contrast of the speckle pattern in the image; and S_{i} is the object image plane.

In a particular case of the coherent image of an object, we have $C_a(\boldsymbol{\delta}) \approx C(\boldsymbol{\delta}) \approx 1$ and $\eta_c \approx 1/(MN)$. The same expression was used in papers [4, 5] to estimate the closeness of the intensity distribution in the accumulated image $\langle I(\boldsymbol{\delta})\rangle_i = N^{-1}\sum I(\boldsymbol{\delta}, \boldsymbol{\rho}_{smn})$ and in the ideal image, which represented the object-surface-roughness-averaged intensity distribution $\langle I(\boldsymbol{\delta}, \boldsymbol{\rho}_{sm_0n_0})\rangle_\xi$ in the instantly recorded coherent image of the object probed by radiation from one source. Therefore, the results of experiments on improving the quality of time-averaged and instant images of this object, presented in papers [4, 5], should completely coincide. For example, by improving the quality of the instant coherent image of a planar triangle rough object due to time averaging of the coherent image of this object, we obtain the image coinciding with the ideal one (Fig. 7).

Figure 7. Improved image of a plane triangular rough object obtained by accumulating statistically independent coherent images formed by simultaneous probing the object by several sources: (*1*) initial coherent object image consisting of seven contrast spots; (*2*) its improved image formed by accumulating ten statistically independent coherent images.

6. Conclusions

(i) The temporal analysis of optical images of a rough object allows one to find the relation between the chromatic properties of probe radiation and coherent properties of optical images of rough nonplanar objects. Thus, if the coherence length L_c of probe radiation exceeds the depth L_s of the backward scattering region of the object, the probe radiation behaves as monochromatic radiation, while the image as a whole manifests itself as a coherent image. If, however, $L_c < L_s$, the probe radiation on the smooth slopes of the object surface behaves as monochromatic radiation, and the image of smooth slopes manifests itself as a coherent image. Under the same condition, the probe radiation on steep slopes behaves as quasi-monochromatic or polychromatic radiation, while the image of steep slopes manifests itself as partially coherent or incoherent radiation.

(ii) The temporal approach can be used for the three-dimensional imaging of rough nonplanar objects by the contrast of speckles in the intensity distribution at different points of their planar optical images, which is determined by using several probe radiation sources.

(iii) This approach allows one to substantiate the method for improving the quality of optical images of a rough object by reducing the contrast of speckles distorting them by means of the simultaneous probing of the object by radiation from several sources with the same average wavelength and arbitrary coherence length. In this case, the distance between sources is chosen so that the images formed with their help would be statistically independent.

Appendix. Calculation of the speckle contrast in an optical image

We will determine the contrast $C_\xi(\boldsymbol{\delta})$ by assuming that the field $E(\boldsymbol{\delta}, t)$ has the Gaussian distribution. In this case,

$$\langle \bar{I}^2(\boldsymbol{\delta})\rangle_\xi \equiv \frac{1}{T^2}\int_{t_0}^{t_0+T}\int_{t_0}^{t_0+T}\langle |E(\boldsymbol{\delta}, t_1)|^2 |E(\boldsymbol{\delta}, t_2)|^2\rangle_\xi \mathrm{d}t_1\mathrm{d}t_2$$

$$= \langle \bar{I}(\boldsymbol{\delta})\rangle_\xi^2 + \frac{1}{T^2}\int_{t_0}^{t_0+T}\int_{t_0}^{t_0+T}|\langle E(\boldsymbol{\delta}, t_1)E^*(\boldsymbol{\delta}, t_2)\rangle_\xi|^2 \mathrm{d}t_1\mathrm{d}t_2$$

$$+ \frac{1}{T^2}\int_{t_0}^{t_0+T}\int_{t_0}^{t_0+T}|\langle E(\boldsymbol{\delta}, t_1)E(\boldsymbol{\delta}, t_2)\rangle_\xi|^2 \mathrm{d}t_1\mathrm{d}t_2.$$

Because the third term in the right-hand side of this expression can be neglected if $\sigma_\xi \gg \lambda_0$ [4], we have

$$\langle \bar{I}^2(\boldsymbol{\delta})\rangle_\xi \approx \langle \bar{I}(\boldsymbol{\delta})\rangle_\xi^2$$

$$+ \frac{1}{T^2}\int_{t_0}^{t_0+T}\int_{t_0}^{t_0+T}|\langle E(\boldsymbol{\delta}, t_1)E^*(\boldsymbol{\delta}, t_2)\rangle_\xi|^2 \mathrm{d}t_1\mathrm{d}t_2.$$

We obtain from this

$$C_\xi(\boldsymbol{\delta}) = \frac{1}{T^2}\int_{t_0}^{t_0+T}\int_{t_0}^{t_0+T}|\langle E_i(\boldsymbol{\delta}, t_1)E_i^*(\boldsymbol{\delta}, t_2)\rangle_\xi|^2 \mathrm{d}t_1\mathrm{d}t_2$$

$$\times \left(\langle \bar{I}(\boldsymbol{\delta})\rangle_\xi^2\right)^{-1}, \tag{A1}$$

where

$$\frac{1}{T^2}\int_{t_0}^{t_0+T}\int_{t_0}^{t_0+T}|\langle E_i(\boldsymbol{\delta}, t_1)E_i^*(\boldsymbol{\delta}, t_2)\rangle_\xi|^2 \mathrm{d}t_1\mathrm{d}t_2$$

$$= \iiiint k(\boldsymbol{r}_1)k^*(\boldsymbol{r}_2)k^*(\boldsymbol{r}_3)k(\boldsymbol{r}_4)h(\boldsymbol{r}_1, \boldsymbol{\delta})h^*(\boldsymbol{r}_2, \boldsymbol{\delta})$$

$$\times h^*(\boldsymbol{r}_3, \boldsymbol{\delta})h(\boldsymbol{r}_4, \boldsymbol{\delta})\Xi(\boldsymbol{r}_1, \boldsymbol{r}_2)\Xi^*(\boldsymbol{r}_3, \boldsymbol{r}_4)\Psi_u(\boldsymbol{r}_1, \boldsymbol{r}_2, \boldsymbol{r}_3, \boldsymbol{r}_4)$$

$$\times F_u(\boldsymbol{r}_1, \boldsymbol{r}_2, \boldsymbol{r}_3, \boldsymbol{r}_4)\mathrm{d}\boldsymbol{r}_1\mathrm{d}\boldsymbol{r}_2\mathrm{d}\boldsymbol{r}_3\mathrm{d}\boldsymbol{r}_4;$$

$$\Xi(\boldsymbol{r}_1, \boldsymbol{r}_2) = \langle \exp\{\mathrm{i}\omega_0 q_N[-\xi(\boldsymbol{r}_1) + \xi(\boldsymbol{r}_2)]/c\}\rangle_\xi;$$

$$\Xi(\boldsymbol{r}_3, \boldsymbol{r}_4) = \langle \exp\{\mathrm{i}\omega_0 q_N[-\xi(\boldsymbol{r}_3) + \xi(\boldsymbol{r}_4)]/c\}\rangle_\xi;$$

$$\Psi_u(\boldsymbol{r}_1, \boldsymbol{r}_2, \boldsymbol{r}_3, \boldsymbol{r}_4) = \exp[\mathrm{i}\omega_0(-2r_1 + \boldsymbol{r}_1\boldsymbol{\rho}_s/r_1 + 2r_2$$

$$- \boldsymbol{r}_2\boldsymbol{\rho}_s/r_2 + 2r_3 - \boldsymbol{r}_3\boldsymbol{\rho}_s/r_3 - 2r_4 + \boldsymbol{r}_4\boldsymbol{\rho}_s/r_4)/c];$$

$$F_u(\boldsymbol{r}_1, \boldsymbol{r}_2, \boldsymbol{r}_3, \boldsymbol{r}_4) = \frac{1}{T^2}\int_{t_0}^{t_0+T}\int_{t_0}^{t_0+T}u(t_1 - 2r_1/c)$$

$$\times u^*(t_2 - 2r_2/c)\, u^*(t_1 - 2r_3/c)\, u(t_2 - 2r_4/c)\mathrm{d}t_1\mathrm{d}t_2$$

$$= B_u[\beta(\boldsymbol{r}_1, \boldsymbol{r}_3)]\, B_u^*[\beta(\boldsymbol{r}_2, \boldsymbol{r}_4)];$$

$$\beta(\boldsymbol{r}_1, \boldsymbol{r}_2) = 2(r_1 - r_2)/L_c.$$

Then, under the condition that $\sigma_\xi \gg \lambda_0$ and the object is probed by coherent radiation with the coherence length $L_c \geqslant L_{cm} = 8\lambda_0 \gg \lambda_0$ [7], we obtain

$$\langle \bar{I}(\boldsymbol{\delta})\rangle_\xi \sim \int k_\xi(\boldsymbol{r})|h(\boldsymbol{r},\boldsymbol{\delta})|^2 \mathrm{d}\boldsymbol{r}, \tag{A2}$$

$$\frac{1}{T^2}\int_{t_0}^{t_0+T}\int_{t_0}^{t_0+T} |\langle E_i(\boldsymbol{\delta},t_1)E_i^*(\boldsymbol{\delta},t_2)\rangle_\xi|^2 \mathrm{d}t_1\mathrm{d}t_2$$

$$\approx \iint k_\xi(\boldsymbol{r}_1)k_\xi(\boldsymbol{r}_2)|h(\boldsymbol{r}_1,\boldsymbol{\delta})h^*(\boldsymbol{r}_2,\boldsymbol{\delta})|^2$$

$$\times |B_u[\beta(\boldsymbol{r}_1,\boldsymbol{r}_2)]|^2 \mathrm{d}\boldsymbol{r}_1\mathrm{d}\boldsymbol{r}_2, \tag{A3}$$

where

$$k_\xi(\boldsymbol{r}) = (\ell_\xi/\sigma_\xi)^2 |\,k(\boldsymbol{r})|^2 \exp(-q_\xi\ell_\xi/\sigma_\xi)^2;$$
$$q_\xi = q_\perp/q_N;\ \ q_\perp \approx (4-q_N^2)^{1/2}. \tag{A4}$$

If the coherence length L_c of probe radiation exceeds the depth of the backward scattering region $L_s \approx (\rho_{cur}\sigma_\xi)/\ell_\xi$ of the object, where ρ_{cur} is the radius of curvature of its surface, then, as shown in [6], we have $|B_u[\beta(\boldsymbol{r}_1,\boldsymbol{r}_2)]|^2 \approx 1$. Then, taking into account relations (A1), (A2), and (A3), we obtain that the contrast of the intensity distribution $\bar{I}(\boldsymbol{\delta})$ in all the regions of the image is unity. In the opposite case, when $L_c \leqslant L_s$, the contrast in each of the regions of the image of a nonplanar object depends on the steepness of the slopes of its surface [4]. The contrast is high in the images of smooth slopes and is low in the images of steep slopes. This means that under the condition $L_c \leqslant L_s$, it is necessary to determine the contrast in the images of different regions of the object surface.

Based on the considerations presented above, we will determine the contrast $C_\xi(\boldsymbol{\delta})$ by fixing a small region of the object and introducing a local rectangular coordinate system $w\,v$ in this region so that the v axis is oriented parallel to the entrance pupil plane of the imaging optical system (Fig. 3). This region almost coincides with a plane tangential to it, which is oriented perpendicular to the normal $\boldsymbol{N}_\xi(\boldsymbol{r})$ to the surface. In this coordinated system, we have $\beta(\boldsymbol{r}_1,\boldsymbol{r}_2) \approx [2q_\xi(w_1-w_2)]/L_c$ [4]. Taking into account this relation and the equality

$$\tau_c = \left|\int_{-\infty}^{\infty} B_u(\tau)\mathrm{d}\tau\right|$$

for the coherence length $L_c \ll L_\xi(\boldsymbol{\delta}) = \Delta_r q_\xi(\boldsymbol{r} = -\mu\boldsymbol{\delta})$, where $L_\xi(\boldsymbol{\delta})$ is the length of the projection of the tangential plane ABCD on the vector $\boldsymbol{q} = 2\boldsymbol{r}_c/r_c$ at a point optically conjugate with the radius vector $\boldsymbol{\delta}$ (see Figs 1 and 3), we will have

$$C_\xi(\boldsymbol{\delta}) = \frac{L_c\Delta_r^2/L_\xi(\boldsymbol{\delta})\int k_\xi^2(\boldsymbol{r})|h(\boldsymbol{r},\boldsymbol{\delta})|^4\mathrm{d}\boldsymbol{r}}{[\int k_\xi(\boldsymbol{r})|h(\boldsymbol{r},\boldsymbol{\delta})|^2\mathrm{d}\boldsymbol{r}]^2}. \tag{A5}$$

References

1. Rigden J.D., Gordon E.F. *Proc. IRE*, **50**, 2367 (1962).
2. Troitskii I.N., Ustinov N.D. *Statisticheskaya teoriya golografii* (Statistical Theory of Holography) (Moscow: Radio i svyaz', 1981).
3. Goodman J. *Statistical Optics* (New York: Wiley&Sons Inc., 2002; Moscow: Mir, 1988).
4. Bakut P.A., Mandrosov V.I., Matveev I.N., Ustinov N.D. *Teoriya kogerentnykh izobrazhenii* (Theory of Coherent Images) (Moscow: Radio i svyaz', 1987).
5. Mandrosov V. *Coherent Fields and Images in Remote Sensing* (Bellingham, WA: SPIE Press, 2004) Vol. PM130.
6. Bakut P.A., Mandrosov V.I. *Kvantovaya Elektron.*, **36**, 239 (2006) [*Quantum Electron.*, **36**, 239 (2006)].
7. Bakut P.A., Mandrosov V.I. *Kvantovaya Elektron.*, **37**, 81 (2007) [*Quantum Electron.*, **37**, 81 (2007)].
8. Mandrosov V.I. *Kvantovaya Elektron.*, **38**, 470 (2008) [*Quantum Electron.*, **38**, 470 (2008)].